Novel Over-current Tripping Device with Multi-level Adjustment Capability Based on Magnetic Coupling for Air Circuit Breakers in DC Traction System

Wen, Weijie; Fan, Jinghan; Li, Bin; Sun, Qingyao; Song, Jinchuan; Popov, Marjan

DOI
10.1109/TPEL.2024.3385354

Publication date
2024

Document Version
Final published version

Published in
IEEE Transactions on Power Electronics

Citation (APA)
Wen, W., Fan, J., Li, B., Sun, Q., Song, J., & Popov, M. (2024). Novel Over-current Tripping Device with Multi-level Adjustment Capability Based on Magnetic Coupling for Air Circuit Breakers in DC Traction System. *IEEE Transactions on Power Electronics*, *39*(10), 12107-12112. https://doi.org/10.1109/TPEL.2024.3385354

Letters

Novel Over-Current Tripping Device With Multilevel Adjustment Capability Based on Magnetic Coupling for Air Circuit Breakers in DC Traction System

Weijie Wen, Jinghan Fan, Bin Li, Qingyao Sun, Jinchuan Song, and Marjan Popov

***Abstract*—In the dc traction power supply system in subway, over-current tripping device (OCTD) is essential for air circuit breakers as backup protection. At present, current threshold value (I_{th}) of OCTD is adjusted by the cooperation of magnetic circuit regulating block (MCRB) and spring. Depending on MCRB is installed or not, only two-level adjustment can be realized, resulting in low adjustment accuracy of I_{th}. In this letter, a novel OCTD based on controllable magnetic coupling is proposed. Instead of using MCRB, an auxiliary winding wrapped on the static iron core is added, with different resistors and thyristors attached. By controlling thyristors, a wide-range and multilevel adjustment of I_{th} can be achieved. Benefits of the proposed method are: reducing the stiffness factor of spring from 55 to 42 N/mm, improving the adjustment accuracy from 0.66 to 0.33 kA/mm, and adjusting I_{th} online without power supply system interruption.**

***Index Terms*—Air circuit breaker (ACB), current threshold value, magnetic coupling, over-current tripping device (OCTD), thyristor module.**

I. Introduction

DC TRACTION power supply system is often used in a subway system. When a short-circuit fault occurs, fault current could reach tens of kiloampere [1], [2], and the typical fault current recorded in field is illustrated in Fig. 1(a). To interrupt the fault current, commercial low-voltage dc breakers (0.75 kV/1.5 kV), mainly provided by GE [3] and Secheron [4], are installed at the outlet of the diode rectifier [5]. Considering air is used as the arc-extinguishing medium [6], this kind of breaker is named as air circuit breaker (ACB) for convenience in this letter.

Manuscript received 12 February 2024; revised 15 March 2024; accepted 31 March 2024. Date of publication 8 April 2024; date of current version 4 September 2024. This work was supported in part by the National Key Research and Development Program of China under Grant 2022YFB2403601, in part by the National Natural Science Foundation of China under Grant 52277120, and in part by the Basic and Applied Basic Research Foundation of Guangdong Province under Grant 2022A1515240068. *(Corresponding authors: Jinghan Fan; Bin Li.)*

Weijie Wen, Jinghan Fan, Bin Li, and Qingyao Sun are with the Key Laboratory of Smart Grid of Ministry of Education and National Industry-Education Platform of Energy Storage, Tianjin University, Tianjin 300072, China (e-mail: fanjh@tju.edu.cn; binli@tju.edu.cn).

Jinchuan Song is with the Tianjin Keyvia Electric Company, Ltd., Tianjin 300392, China.

Marjan Popov is with the Faculty of Electrical Engineering, Mathematics and Computer Science, Delft University of Technology, CD2628 Delft, The Netherlands.

Color versions of one or more figures in this article are available at https://doi.org/10.1109/TPEL.2024.3385354.

Digital Object Identifier 10.1109/TPEL.2024.3385354

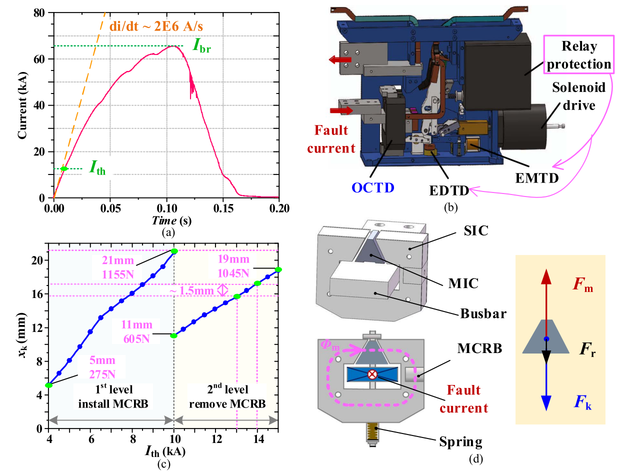

Fig. 1. Full diagram of ACB. (a) Fault current. (b) Physical structure. (c) Output characteristic of existing OCTD. (d) Structure of existing OCTD.

To handle diversified faults with random position or resistance, multiple tripping devices are installed in ACB, including electro-dynamic tripping device (EDTD), electromagnetic tripping device (EMTD), and over-current tripping device (OCTD) [7], [8], as shown in Fig. 1(b). Usually, ACB is tripped by EDTD or EMTD, which receives signals from relay protection [9]. However, both EDTD and EMTD are invalid when relay protection loses power [10]. In addition, the response time of EDTD and EMTD is usually $\geq$10 ms, which is too long for nearby fault. Therefore, OCTD, which is actually a mechanical device controlled by fault current itself and does not rely on relay protection, must be installed as a backup protection to trip ACB when EDTD and EMTD are invalid.

The structure of OCTD is shown in Fig. 1(d), where SIC indicates static iron core, MIC indicates movable iron core, and MCRB indicates magnetic circuit regulating block. The forces applied on MIC are shown in Fig. 1(d), including $F_{\rm m}$, $F_{\rm k}$, and $F_{\rm r}$. $F_{\rm m}$ is the electromagnetic force induced by the fault current; $F_{\rm k}$ is the reaction force provided by the spring; $F_{\rm r}$ is the mechanical drag force. $F_{\rm r}$ is much smaller than $F_{\rm m}$ and $F_{\rm k}$, and can be ignored.

The working principle of OCTD is: when the fault current exceeds $I_{\rm th}$, the induced $F_{\rm m}$ would exceed $F_{\rm k}$, resulting in MIC moves up to trip the separation of contacts inside ACB

[7]. Therefore, I_{th} is determined by the pre-set F_{k}, which is in direct proportion to the compression displacement (x_{k}) of spring. The relationship between x_{k} and I_{th} is defined as the output characteristic of OCTD, just as shown in Fig. 1(c).

In practice, ACB needs to be applied in various dc traction systems, and their loads are different. When a system only has one train running (such as test line), its rated current is only 800–1200 A, and I_{th} should be set lower to ensure the sensitivity of protection. When there are multiple trains running [11], the rated current is higher and maybe close to 4 kA, so I_{th} needs to be set higher to avoid the mis-operation of OCTD caused by current fluctuations. Therefore, I_{th} needs to be adjustable, and its value depends on the load of system.

To meet the needs of different systems, the adjustment range of I_{th} is usually set within 4–15 kA [3]. However, there is a maximum limit for the compression displacement (x_{k}) of spring, and adjusting F_{k} alone cannot achieve such a wide range of I_{th}. Therefore, magnetic circuit regulating block (MCRB) is used to split the range of I_{th} into two levels. The working principle is: in Fig. 1(c), when MCRB is installed, the reluctance of the looped magnetic circuit is relatively small. I_{th} in range of 4–10 kA could generate enough F_{m} to overcome F_{k} in range of 275–1155 N, so that MIC moves up to trip ACB, forming the first level of I_{th}. When MCRB is removed, the reluctance of the looped magnetic circuit increases. Larger I_{th} in the range of 10–15 kA is needed to generate F_{m} to overcome F_{k} in the range of 605–1045 N, forming the second level of I_{th}.

According to Fig. 1(c), in existing OCTD, the maximum force of spring should be not less than 1155 N. Due to space limitation inside ACB, the spring must have a high stiffness factor k to ensure x_{k} within limits, meaning the adjustment accuracy of I_{th} is quite low. For example, to adjust I_{th} from 13 to 14 kA, x_{k} of spring should increase by $\sim$1.5 mm, meaning the adjustment accuracy is 0.66 kA/mm. In practice, the spring is compressed manually, and it is very difficult to obtain accurate I_{th} within such a small interval. In addition, to save space inside ACB, the maximum allowable force provided by spring is only $\sim$1200 N. Referring to Fig. 1(c), when I_{th} of 10 kA is desired, the spring has to be compressed near limits for a long time to provide 1150 N, meaning plastic deformation may occur and cause random changes of k and F_{k}, further aggravating the error. Another problem is in practical use, MCRB is manually screwed ON or OFF, meaning the adjustment has to be offline, which is quite inconvenient.

To tackle these problems, a novel OCTD based on magnetic coupling is proposed in this letter. By adding auxiliary winding (AW) with thyristors and resistors attached, a multilevel adjustment of I_{th} can be achieved by controlling thyristors. The research is validated by thorough theoretical analysis, simulation and experiments.

II. Proposed OCTD

A. Possible Multilevel Adjustment Methods of I_{th} in OCTD

To find better method to realize multilevel wide-range adjustment of I_{th}, basic working principle of possible multilevel adjustment methods is discussed to guide the design of novel OCTD.

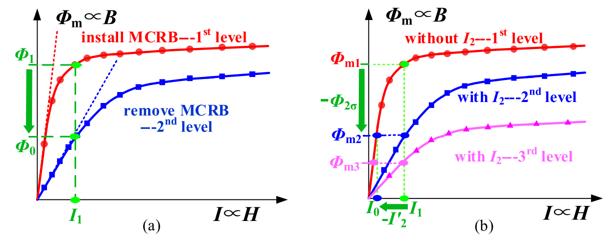

Fig. 2. Multilevel adjustment of I_{th} in OCTD. (a) Changing magnetic circuit by MCRB. (b) Changing electrical circuit by adding AW.

Referring to Fig. 1(d), based on Ampere circuit law, the magnetic flux (Φ_{m}) in looped magnetic circuit can be expressed as (1), where n_1 (=1) is the turn of current through busbar; I_1 is the current through busbar; R_{m} is the total reluctance of looped magnetic circuit, and it consists of four components: $R_{\mathrm{SIC}}, R_{\mathrm{MIC}}, R_{\mathrm{MCRB}}$, and R_{gap}, indicating the reluctance of SIC, MIC, MCRB, and air gap between SIC and MIC.

$$\phi_{\mathrm{m}} = \frac{n_1 \cdot I_1}{R_{\mathrm{m}}} = \frac{n_1 \cdot I_1}{R_{\mathrm{SIC}} + R_{\mathrm{MIC}} + R_{\mathrm{gap}} + R_{\mathrm{MCRB}}} \tag{1}$$

$$\phi_{\mathrm{m}} = \oint B \cdot dS \;\Rightarrow\; \phi_{\mathrm{m}} \propto B,$$

$$n_1 \cdot I_1 = \oint H \cdot dl \Rightarrow \; I_1 \propto H. \tag{2}$$

With physical dimensions of OCTD determined, $\Phi_{\mathrm{m}} \propto B$; $I_1 \propto H$, just as shown in (2), where S is the integration area of B (magnetic induction intensity); l is the integration path of H (magnetic field strength). Therefore, the relationship curve of ($\Phi_{\mathrm{m}} \sim I_1$) has the same shape with ($B \sim H$), just as shown in Fig. 2.

The induced electromagnetic force (F_{m}) applied on MIC can be expressed as (3), where μ_0 is the permeability of air gap between SIC and MIC, showing $F_{\mathrm{m}} \propto {\Phi_{\mathrm{m}}}^2$. Therefore, if the relationship curve of ($\Phi_{\mathrm{m}} \sim I_1$) is variable, multilevel adjustment of I_{th} can be realized.

$$F_{\mathrm{m}} = \int \frac{\vec{B} \cdot \vec{H}}{\mu_0} \cdot dS \Rightarrow F_{\mathrm{m}} \; \propto {\phi_m}^2. \tag{3}$$

In existing OCTD, referring to (1), when MCRB is installed or removed, variable R_{m} is obtained, and the relationship curve of ($\Phi_{\mathrm{m}} \sim I_1$) is the red line or blue line in Fig. 2(a). With MCRB installed or removed, the induced Φ_{m} by the same current (I_1) varies from Φ_1 to Φ_0, meaning different F_{m} is generated, and the wide range of I_{th} is split into two levels.

Referring to (1), except for changing R_{m} by magnetic circuit, another method to change the relationship curve of ($\Phi_{\mathrm{m}} \sim I_1$) is to add an AW wrapped on SIC. In this case, (1) changes to (4), where n_2 is the turn of AW; I_2 is the current through AW.

$$\phi_{\mathrm{m}} = \phi_1 - \phi_2 = \frac{n_1 \cdot I_1 - n_2 \cdot I_2}{R_{\mathrm{m}}} = \frac{n_1 \cdot I_1 - n_2 \cdot I_2}{R_{\mathrm{SIC}} + R_{\mathrm{MIC}} + R_{\mathrm{gap}}}. \tag{4}$$

By controlling n_2 and I_2 properly, more than two levels of adjustment of I_{th} could be realized, which is helpful to improve

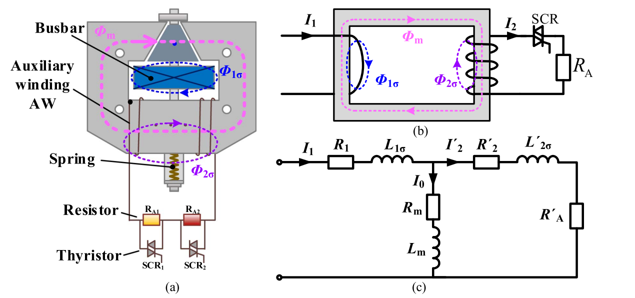

Fig. 3. Novel OCTD. (a) Structure. (b) Magnetic fluxes. (c) Equivalent circuit.

the adjustment accuracy of I_{th}. Starting from this unique perspective, a novel OCTD is proposed by us.

B. Novel OCTD Based on Magnetic Coupling

Structure and equivalent circuit of the proposed OCTD are shown in Fig. 3. Instead of MCRB, AW wrapped around SIC is added. Bidirectional thyristors (SCR) and resistors (R_{A}) are connected to the two terminals of AW.

In Fig. 3, I_1 and I_2 indicate the current through busbar and AW, respectively; Φ_{m}, $\Phi_{1\sigma}$, and $\Phi_{2\sigma}$, respectively, indicate the main magnetic flux hinged with I_1 and I_2, leakage magnetic flux only hinged with I_1, and leakage magnetic flux hinged only with I_2.

Taking busbar as the primary winding with turn of $n_1 = 1$ and AW as the secondary winding with turn of n_2 of a transformer, the equivalent circuit of novel OCTD is derived as shown in Fig. 3(c), where L_{m}, $L_{1\sigma}$, and $L'_{2\sigma}$ are the equivalent inductance of Φ_{m}, $\Phi_{1\sigma}$, and $\Phi_{2\sigma}$, respectively, looking from busbar side; R_{m}, R_1, and R'_2 are the equivalent resistance of iron core, busbar, and AW, respectively, looking from busbar side. R'_{A} is the equivalent additional resistance in AW, looking from busbar side. In this case, the mathematical relationship between I_1 and I_2 can be expressed by

$$
\begin{aligned}
I_1 &= I_0 + I'_2; \qquad L_{\mathrm{m}} \cdot \frac{dI_0}{dt} = L'_{2\sigma} \cdot \frac{dI'_2}{dt} + I'_2 \cdot (R'_{\mathrm{A}} + R'_2) \\
I'_2 &= (n_2/n_1) \cdot I_2; \quad L'_{2\sigma} = (n_1/n_2)^2 \cdot L_{2\sigma}; \\
& (R'_{\mathrm{A}} + R'_2) = (n_1/n_2)^2 \cdot (R_{\mathrm{A}} + R_2).
\end{aligned} \tag{5}
$$

The working principle of the OCTD is: when SCR_1 and SCR_2 are OFF-state, the total resistance of AW is $(R_{\mathrm{A1}} + R_{\mathrm{A2}} + R_2)$, I_2 is almost zero, and F_{m} applied on MIC is determined by Φ_{m1}, which is induced only by I_1, forming the first level of I_{th} in Fig. 2(b). When only SCR_1 is ON-state, the total resistance of AW is $(R_{\mathrm{A2}} + R_2)$; along with the rapid increase of I_1 due to the fault occurrence, relatively larger I_2 would be induced, and F_{m} applied on MIC is determined by Φ_{m2}, which is induced by I_1 and I'_2, forming the second level of I_{th} in Fig. 2(b). When SCR_1 and SCR_2 are both ON-state, the total resistance of AW is R_2; larger I_2 would be induced and F_{m} applied on MIC is determined by Φ_{m3}, forming the third level of I_{th} in Fig. 2(b). Therefore, by controlling different thyristors, three-level resistance of AW can be obtained to generate different I_2, so that three-level adjustment of I_{th} can be realized online easily. It should be noted that more levels of adjustment of I_{th} can be realized by using more thyristors if needed.

Without changing the dimension of SIC and MIC, parameters of AW to be determined are R_{A} and n_2, and they can be obtained by the following steps.

Step 1: Critical values of first-level I_{th} are classified as $I_{\mathrm{th\_1min}}$ (lower limit) and $I_{\mathrm{th\_1max}}$ (upper limit). F_{m}, induced by I_1 and I'_2, should be less than $F_{\mathrm{k\_max}}$ (the maximum allowable force provided by spring). Therefore, regarding I'_2 to be almost zero, $I_{\mathrm{th\_1max}}$ can be designed according to $F_{\mathrm{k\_max}}$; $I_{\mathrm{th\_1min}}$ is designed to be the lower limit of I_{th} (4 kA).

Step 2: After $I_{\mathrm{th\_1max}}$ is determined, I'_2 for each level can be selected. For the first level ($I_{\mathrm{th}} \leq I_{\mathrm{th\_1max}}$), no I'_2 is required; for the second level, when $I_{\mathrm{th}} > I_{\mathrm{th\_1max}}$ is desired, I'_2 is needed to ensure F_{m} (induced by I_1 and I'_2) $\leq F_{\mathrm{k\_max}}$. Therefore, the upper and lower limit of second level ($I_{\mathrm{th\_2}}$) can be determined by (6). Similarly, the upper and lower limit of third level ($I_{\mathrm{th\_3}}$) can also be determined by

$$
\begin{aligned}
& I_{\mathrm{th\_2max}} - I'_2 \leq I_{\mathrm{th\_1max}}; \quad I_{\mathrm{th\_2min}} = I_{\mathrm{th\_1max}} \\
& I_{\mathrm{th\_3max}} - I'_2 \leq I_{\mathrm{th\_1max}}; I_{\mathrm{th\_3min}} = I_{\mathrm{th\_2max}}.
\end{aligned} \tag{6}
$$

To obtain specific parameters of AW, R_{A} and n_2 should be designed to obtain the required I'_2. Because $L_{2\sigma}$ is proportional with $(n_2)^2$, referring to (5), the induced I'_2 looking from busbar side is irrelevant with n_2. With different n_2, I_2 in AW is different, but I'_2 looking from busbar side is the same. Therefore, n_2 can be designed by considering other factors such as manufacture difficulty and current limit of AW.

With dimensions of SIC, MIC unchanged, L_{m}, $L'_{1\sigma}$, R_1, and R_{m} are determined, and they can be extracted by simulation based on finite element method. Once n_2 and the cross-sectional area of AW are determined, $L'_{2\sigma}$ and R'_2 are also determined, and they can be extracted by simulation. Referring to the value of I'_2 in (6), the value of $(R'_2 + R'_{\mathrm{A}})$ can be calculated by (5). Then, taking n_2 into consideration, the actual value of R_{A} can be obtained to split the range of I_{th} into multilevel. Within each level, x_{k} of spring is adjusted to ensure F_{m} (induced by I_{th} and I'_2) is equal to F_{k}.

In conclusion, rough multilevel adjustment of I_{th} is realized by controlling SCRs in AW; fine adjustment of I_{th} within each level is realized by adjusting x_{k} of spring.

III. Simulation of the Novel OCTD

A. Model Parameters

Finite element simulation model of novel OCTD is established in ANSYS. The physical dimensions of SIC and MIC are shown in Fig. 4, and the depth of model is 50 mm. Its parameters are designed by the method described in Section II-B. Taking the three-levels as an example, the range of I_{th} is divided as first level (4–7 kA), second level (7–10 kA), third level (10–15 kA), meaning I'_2 is 3 and 9 kA for second level and the third level, respectively.

As for AW, n_2 is set to be 20, the diameter of copper wire is 2 mm, and $R_2 = 0.01\ \Omega$. Inductance has been extracted by

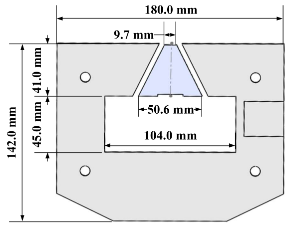

Fig. 4. Physical dimensions of SIC and MIC.

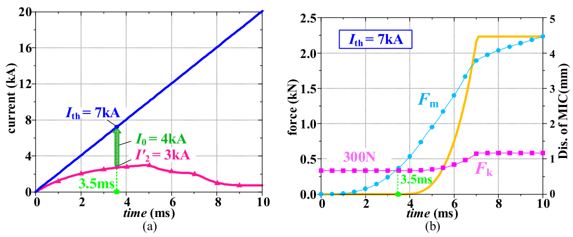

Fig. 5. Simulation results. (a) Currents. (b) Forces and displacement of MIC.

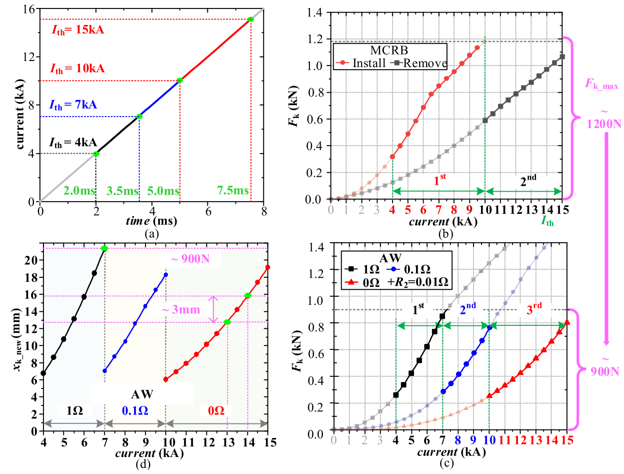

Fig. 6. Simulated output characteristics of existing OCTD and novel OCTD. (a) Fault current. (b) F_k for different I_{th} in existing OCTD. (c) F_k for different I_{th} in novel OCTD. (d) Output characteristic of novel OCTD.

simulation in advance ($L_m = 4.7$E-7H, $L'_{2\sigma} = 7.12$E-8H, and $L_{1\sigma}$ is almost zero). To simulate nearby fault, I_1 rises up from 0 kA with a rate of 2 kA/ms, as shown in Fig. 5(a). Referring to (5), $R_{A1} + R_{A2}$ is 1 Ω and R_{A2} is 0.1 Ω, forming three-level resistance of $(1 + R_2)$, $(0.1 + R_2)$, and (R_2), which corresponds to three levels of I_{th}.

B. Simulation Results

Taking $I_{th} = 7$ kA in second level as an example, by setting F_k to 300 N, simulation results of currents, forces, and displacement of MIC during the whole tripping process are shown in Fig. 5.

As shown in Fig. 5(a), when I_1 reaches $I_{th} = 7$ kA at 3.5 ms, the induced current I'_2 in AW reaches 3 kA, and according to (5), I_0 increases to 4 kA. As F_m is decided by I_0, F_m increases along with the increase of I_0, and it reaches F_k at $t = 3.5$ ms, resulting in MIC starts moving.

It should be noted that x_k and F_k also increases with the moving of MIC. But F_m rises faster than F_k, resulting in MIC can move up continuously to the terminal position (4.5 mm) to trip the separation of contacts inside ACB. Therefore, setting the resistance of AW to $(0.1 + R_2)$ to form the second level, I_{th} can be adjusted to 7 kA by setting required F_k of 300 N.

For comparison, simulation results of the existing OCTD using MCRB and the novel OCTD using AW are shown in Fig. 6. Relationships between I_{th} and F_k for the existing OCTD and the novel OCTD are presented in Fig. 6(b) and (c), respectively. By splitting more levels in novel OCTD, F_{k_max} (maximum force of spring) is reduced from ∼1200 to ∼900 N. With same space, k of the spring can be designed as 42 N/mm instead of 55 N/mm, and the output characteristic of the novel OCTD is shown in Fig. 6(d).

Comparing Figs. 1(c) and 6(d), when adjusting I_{th} from 13 to 14 kA, x_k of the spring increases by 3 mm, meaning the adjustment accuracy is 0.33 kA/mm, better than 0.66 kA/mm in Fig. 1(c). Simulation results proved that the novel OCTD can reduce the stiffness factor of spring, improve the adjustment accuracy, and adjust I_{th} online without power system interruption.

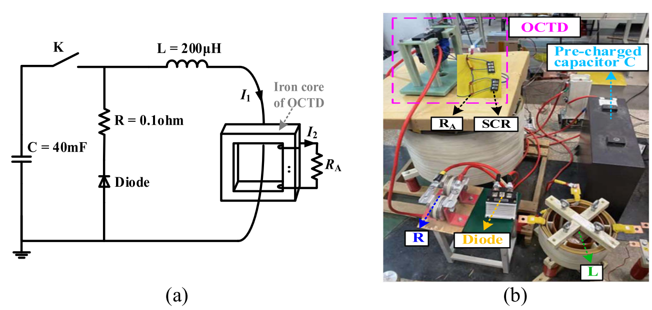

Fig. 7. Experimental test. (a) Test circuit. (b) Picture.

IV. Experimental Verifications

Experimental platform is shown in Fig. 7. The busbar current (I_1) is generated by a precharged capacitor (C) through an inductor (L). A freewheel branch (resistor R and Diode) is used to reduce the decreasing rate of I_1 after its peak. The part number of SCR is MFX110A. Tests were carried out with different I_1 by setting different recharged voltage on C. The movement of MIC is observed by high-speed camera. I_1 and I_2 are measured by Rogowski coils.

As the maximum voltage applied on C is 1 kV, the maximum current of I_1 produced in our lab is ∼9 kA. To verify the proposed OCTD, F_k is set to be 100 N in tests, and experimental results are shown in Fig. 8.

As shown in Fig. 8(a), for the first level ($R_A = 1\Omega$), MIC starts moving when I_1 is 2.8 kA, $I'_2 = 0.8$ kA, and $I_0 = I_1$-I'_2 = 2.0 kA. After 1.6 ms, MIC moves over 1 mm (when its top coincides with the top of SIC). After 2.1 ms, MIC moves to the terminal position of 4.5 mm, which is enough to trip ACB. As shown in Fig. 8(b), for the second level ($R_A = 0.1$ Ω), MIC starts moving when I_1 is 5.3 kA; as shown in Fig. 8(c), for 3rd level ($R_A = 0$ Ω), MIC starts moving when I_1 is 7 kA. In all the three

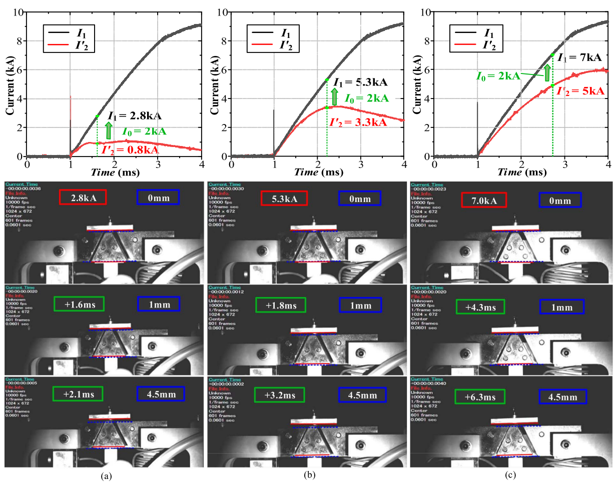

Fig. 8. Experimental results. (a) First level. (b) Second level. (c) Third level.

levels, I_0 is the same (2.0 kA), generating same F_m to overcome F_k. Therefore, by setting different R_A, the same F_k corresponds with different I_th (2.8 kA, 5.3 kA, 7 kA), validating the proposed OCTD.

According to Fig. 6(c) in Section III, when $F_\mathrm{k} = 100$ N, the simulation results of I_th for three levels are (2.3 kA, 4.9 kA, 7 kA), which derives a little from the experimental results (2.8 kA, 5.3 kA, 7 kA). The reasons for the deviations are: 1) in experiments, frames per second of the high-speed camera is 10 k/s, meaning only one picture is recorded in 0.1 ms. Besides, the initial movement of MIC is slight, and measurement error of the initial movement time of MIC is inevitable, leading to a measurement error of I_th in experiments. 2) The fault current in the experiment is generated by the discharge of precharged capacitor, and its rising rate ($\mathrm{d}I_1/\mathrm{d}t$) is variable. Differently, the $\mathrm{d}I_1/\mathrm{d}t$ in simulation is constant before ACB tripping, which is consistent with the practical fault current shown in Fig. 1. The difference of $\mathrm{d}I_1/\mathrm{d}t$ would induce different current through AW, causing changes in I_th.

It should be noted that different $\mathrm{d}I_1/\mathrm{d}t$ can only cause slight changes in I_th. The reason is that OCTD is a backup protection to trip ACB, and it usually deals with nearby faults at the outlet of rectifier. In this case, $\mathrm{d}I_1/\mathrm{d}t$ is usually less than 2 kA/ms [4], which is decided by the time constant of faulty circuit. Taking $\mathrm{d}I_1/\mathrm{d}t = 1$ kA/ms and 2 kA/ms as examples, when assuming $I_\mathrm{th} = 4$ kA, the time for I_1 to reach I_th (Δt) is 4 and 2 ms, respectively. Referring to (5), if the resistance is neglected, $\mathrm{d}I'_2/\mathrm{d}t$ is proportional with $\mathrm{d}I_1/\mathrm{d}t$, the induced current ($I'_2 = \mathrm{d}I'_2/\mathrm{d}t \times \Delta t$) through AW is the same, resulting in same I_0 ($= I_1$-I'_2) and generating same F_m. However, in practice, the resistance cannot be neglected completely, meaning it would cause slight changes of I_th under different $\mathrm{d}I_1/\mathrm{d}t$. Still taking $F_\mathrm{k} = 100$ N as an example, simulation results of I_th for three levels are (2.3 kA, 4.7 kA, 7 kA) when $\mathrm{d}I_1/\mathrm{d}t = 1$ kA/ms, and (2.3 kA, 4.9 kA, 7 kA) when $\mathrm{d}I_1/\mathrm{d}t = 2$ kA/ms. Therefore, the change in I_th brought by the variation of $\mathrm{d}I_1/\mathrm{d}t$ is relatively small.

Apart from the tests with fixed F_k (= 100 N), two other tests were also carried out, with $F_\mathrm{k} = 400$ N set in the first level and

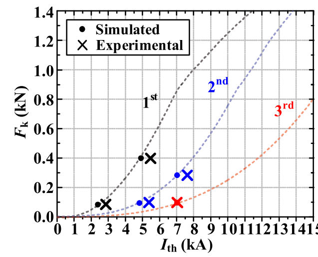

Fig. 9. Comparison of simulation results and experimental results.

$F_\mathrm{k} = 300$ N set in the second level, as shown in Fig. 9. The experimental results are quite consistent with the simulations, validating the proposed OCTD.

V. Performance Comparison

To present the superiority of the proposed OCTD over the existing OCTD, performance comparisons in terms of adjustment range and accuracy are conducted in this section.

According to Fig. 6(b) and (c), $F_\mathrm{k\_max}$ is ∼1200 N for the existing OCTD and ∼900 N for the proposed OCTD. By splitting the total range of I_th into multiple levels, $F_\mathrm{k\_max}$ is effectively reduced, and the spring is no longer compressed near its limit. This can extend the service time of spring, improve the accuracy of F_k, and enable a wider range of adjustment with a same spring.

The reduction in $F_\mathrm{k\_max}$ also enables the spring with lower k (stiffness factor) to be used for a same adjustment range. Comparing Figs. 1(c) and 6(d), k is 55 N/mm for the existing OCTD and 42 N/mm for the proposed OCTD. With lower k, the proposed OCTD can improve the adjustment accuracy from 0.66 to 0.33 kA/mm. This provides larger intervals for manual adjustment of spring, contributing to the adjustment accuracy.

VI. Conclusion

Instead of using MRCB, a novel OCTD based on magnetic coupling effect is proposed in this letter. By controlling different thyristors, magnetic coupling effect is controllable to realize multilevel wide-range OCTD. Theoretical analysis, simulation based on finite element method, and experiments are carried out to validate the proposed OCTD. Compared with the existing OCTD, the proposed OCTD can reduce the stiffness factor of spring from 55 to 42 N/mm, improve the adjustment accuracy from 0.66 to 0.33 kA/mm, and adjust I_th online without power supply system interruption.

References

[1] E. Pons, P. Colella, R. Rizzoli, and R. Tommasini, "Optimization of digital overcurrent protection settings in DC Urban Light Railway systems," *IEEE Trans. Ind. Appl.*, vol. 55, no. 4, pp. 3437–3444, Jul./Aug. 2019, doi: 10.1109/TIA.2019.2914415.

[2] J. S. Morton, "Circuit breaker and protection requirements for DC switchgear used in rapid Transit systems," *IEEE Trans. Ind. Appl.*, vol. IA-21, no. 5, pp. 1268–1273, Sep. 1985, doi: 10.1109/TIA.1985.349553.

[3] GE Consumer & Industrial, "Gerapid 2607 user manual - High speed DC circuit breaker," GE Consumer Industrial, Boston, MA, USA, 2010. [Online]. Available: https://www.manualsdir.com/manuals/295789/ge-industrial-solutions-gerapid-2607-4207-6007-8007-with-arc-chutes-1x2-1x4-2x2-2x3-2x4.html

[4] Sécheron SA, “DC circuit breakers,” 2020. [Online]. Available: https://www.secheron.com/wp-content/uploads/docs/SG104136BEN_C04_Brochure_Circuit-breaker-DC_UR10-15_08.20.pdf
[5] Y. Chen, Z. Tian, C. Roberts, S. Hillmansen, and M. Chen, “Reliability and life evaluation of a DC traction power supply system considering load characteristics,” *IEEE Trans. Transp. Electrific.*, vol. 7, no. 3, pp. 958–968, Sep. 2021, doi: 10.1109/TTE.2020.3047512.
[6] C. Mondellini, M. Corna, and L. Stendardi, “High speed circuit breaker for industrial and railways applications, ” U.S. Patent 11 004 625, May 11, 2021.
[7] B. Li, D. Chen, J. He, C. Wang, J. Song, and H. Lyu, “Fault analysis and protection in flexible DC traction power supply system,” *IEEE Trans. Transp. Electrific.*, early access, doi: 10.1109/TTE.2023.3322322.
[8] Q. Huo, J. Xiong, N. Zhang, X. Guo, L. Wu, and T. Wei, “Review of DC circuit breaker application,” *Electric Power Syst. Res.*, vol. 209, Mar. 2022, Art. no. 107946, doi: 10.1016/j.epsr.2022.107946.
[9] M. Bartosik, P. Borkowski, E. Raj, and F. Wójcik, “The new Family of low-voltage, hyper-speed arcless, hybrid, DC circuit breakers for urban traction vehicles and related industrial applications,” *IEEE Trans. Power Del.*, vol. 34, no. 1, pp. 251–259, Feb. 2019, doi: 10.1109/TPWRD.2018.2884623.
[10] M. Berger, J.-P. M. Grave, C. Lavertu, I. Kocar, J. Mahseredjian, and D. Ferrara, “Modeling, simulation, and testing of switching surge transients in rapid transit vehicles DC power systems,” *IEEE Trans. Ind. Appl.*, vol. 54, no. 1, pp. 822–831, Jan./Feb. 2018, doi: 10.1109/TIA.2017.2761870.
[11] H. Yu, G. Zhang, R. Wang, and W. Xiong, “A real-time adaptive energy optimization method for urban rail flexible traction power supply system,” *IEEE Trans. Intell. Transp. Syst.*, vol. 24, no. 9, pp. 10155–10164, Sep. 2023, doi: 10.1109/TITS.2023.3271129.